Cortical thickness or grey matter volume? The importance of selecting the phenotype for imaging genetics studies

Anderson M. Winkler [a,b,*], Peter Kochunov [c], John Blangero [d], Laura Almasy [d], Karl Zilles [e,f], Peter T. Fox [c], Ravindranath Duggirala [d], David C. Glahn [a,b,c]

[a] Department of Psychiatry, Yale University School of Medicine, New Haven, CT, USA
[b] Olin Neuropsychiatry Research Center, The Institute of Living, Hartford, CT, USA
[c] Research Imaging Center, University of Texas Health Science Center at San Antonio, San Antonio, TX, USA
[d] Department of Genetics, Southwest Foundation for Biomedical Research, San Antonio, TX, USA
[e] Institute of Neuroscience and Medicine (IMN-2), Research Center Jülich, Jülich, Germany
[f] C. & O. Vogt-Institut fur Hirnforschung, Heinrich Heine Universität, Düsseldorf, Germany

ABSTRACT

Choosing the appropriate neuroimaging phenotype is critical to successfully identify genes that influence brain structure or function. While neuroimaging methods provide numerous potential phenotypes, their role for imaging genetics studies is unclear. Here we examine the relationship between brain volume, grey matter volume, cortical thickness and surface area, from a genetic standpoint. Four hundred and eighty-six individuals from randomly ascertained extended pedigrees with high-quality T1-weighted neuroanatomic MRI images participated in the study. Surface-based and voxel-based representations of brain structure were derived, using automated methods, and these measurements were analysed using a variance-components method to identify the heritability of these traits and their genetic correlations. All neuroanatomic traits were significantly influenced by genetic factors. Cortical thickness and surface area measurements were found to be genetically and phenotypically independent. While both thickness and area influenced volume measurements of cortical grey matter, volume was more closely related to surface area than cortical thickness. This trend was observed for both the volume-based and surface-based techniques. The results suggest that surface area and cortical thickness measurements should be considered separately and preferred over gray matter volumes for imaging genetic studies.

© 2009 Elsevier Inc. All rights reserved.

Introduction

Despite evidence that most neurological and psychiatric illnesses are genetically mediated, the identification of genes that predispose brain-related disorders has been difficult. One strategy for unraveling the genetic determinants of these complex illnesses is the use of endophenotypes, also called intermediate phenotypes (Gottesman and Shields, 1967; Gottesman and Gould, 2003), which are quantitative traits that are genetically correlated with illness. Neuroimaging methods provide an array of potential endophenotypes for these disorders (Glahn et al., 2007). Although there is mounting evidence that quantitative indices derived from brain structure and function are heritable (Baaré et al., 2001; Thompson et al., 2001; Geschwind et al., 2002; Peper et al., 2007; Glahn et al., 2007), and associated with neuropsychiatric disorders (McDonald et al., 2006; Honea et al., 2008; Goldman et al., 2008, 2009; van der Schot et al., 2009), it is unclear

which genes influence these traits or the biological mechanisms that govern these measurements. The search for genes that influence brain-related traits could be improved by choosing imaging phenotypes that are closest to a single gene action (Wojczynski and Tiwari, 2008). However, given the complexity and multi-dimensional nature of imaging data, it is critical to determine the appropriate measurements to be employed. In this report, we examine issues surrounding the use of imaging-derived grey matter measurements in imaging genetics studies.

Although the human brain is gyrencephalic, with no absolute linear relationship between brain volume and surface area (Hofman, 1985; Armstrong et al., 1995), simple geometric laws still hold within the cortical mantle, where the grey matter volume is defined as the amount of grey matter that lies between the grey-white interface and the pia mater (Fig. 1, left). Previous findings suggest that cortical surface area and cortical thickness are independent, both globally and regionally, that grey matter volume is a function of these two indices and each of these three measurements are heritable (Winkler et al., 2009; Panizzon et al., 2009). Furthermore, Panizzon et al. (2009) reported that surface area and cortical thickness are genetically uncorrelated. Thus, volume measurements, which combine aspects of

* Corresponding author. Department of Psychiatry, Yale University School of Medicine, New Haven, CT, USA.
E-mail address: anderson.winkler@yale.edu (A.M. Winkler).
URL: http://www.glahngroup.org (D.C. Glahn).

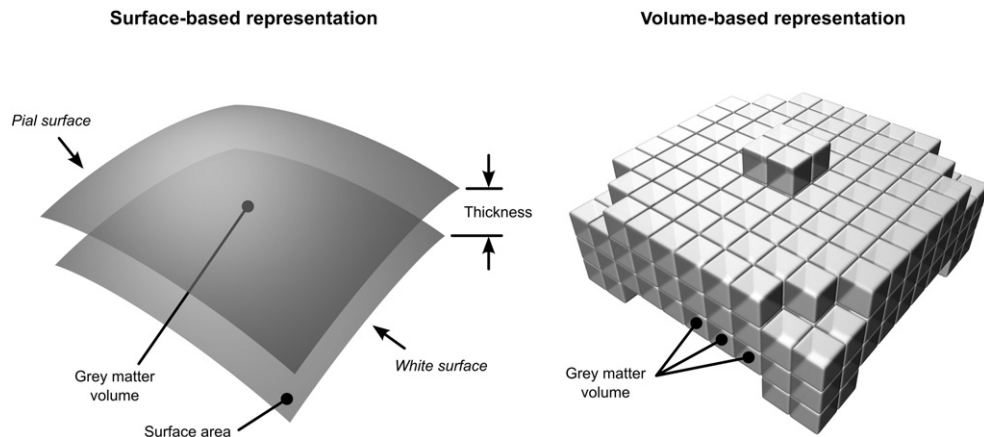**Surface-based representation**   **Volume-based representation**

Fig. 1. Geometrical relationship between cortical thickness, surface area and grey matter volume. In the surface-based representation, the grey matter volume is a quadratic function of distances in the surfaces and a linear function of the thickness. In the volume-based representation, only the volumes can be measured directly and require partial volume-effects (not depicted) to be considered.

both traits, are likely influenced by some combination of these genetic factors. Since different definitions of a phenotype potentially lead to different genetic findings (Rao, 2008), it would seem that surface or thickness measures would have advantages over volume measures for gene discovery.

Cortical anatomy, which is structured as a corrugated two-dimensional sheet of tissue, can be well represented by surface models, which facilitate the analysis of relationships between cortical regions and provide superior visualisation (van Essen et al., 1998). Intersubject and even interspecies registration can be accomplished using surface-based representations (van Essen et al., 2001), allowing matching of homologies without relying directly on spatial smoothing as in volume-based methods (Ashburner and Friston, 2000). Computational advances in surface reconstruction (Mangin et al., 1995; Dale et al., 1999; Fischl et al., 1999a) and the availability of software packages also facilitates its use. Despite these advantages, quantitative methods based on purely volumetric representations of the brain are still common. Amongst these, voxel-based morphometry (VBM) (Wright et al., 1995; Bullmore et al., 1999; Ashburner and Friston, 2000; Good et al., 2001) is a relatively fast, straightforward method, that quantifies the amount of grey matter existing in a voxel and permits a comparison across subjects (Fig. 1, right). VBM requires that voxels are classified according to different tissue types, usually grey matter, white matter and cerebrospinal fluid (GM/WM/CSF). To allow comparison across subjects, images are non-linearly aligned to a standard brain, where a common coordinate system can be defined, and volumes are corrected for local shrinkages and expansions using the Jacobian determinants of the warps at each voxel (Good et al., 2001). In this way, VBM allows for the quantification of the grey matter volumes, globally and regionally, using either the voxels directly or regions of interest.

In this study, we compare measurements obtained with VBM methods, with measurements from surface-based representations of the brain in genetically informative samples. We focus our attention to determining the genetic control over (1) the volume of the grey matter computed using surface-based and volume-based representations of the brain, (2) the cortical surface area and (3) the cortical thickness.

Methods

Participants

Subjects participated in the Genetics of Brain Structure and Function Study, GOBS, a collaborative effort involving the Southwest Foundation for Biomedical Research, the University of Texas Health Science Center at San Antonio (UTHSCSA) and the Yale University School of Medicine. To date, more than 1000 individuals from randomly selected families of Mexican-American ascent, who live in San Antonio, Texas, USA, have been recruited. The data presented here is based on the analysis of the T_1-weighted MRI images from the 486 subjects scanned before December 31st, 2008. A summary of the pedigree structure is presented in Table 1. The mean age of this group was 48.6 ± 13.2 years (min = 26.1, max = 85.1) and 302 were females. All participants provided written informed consent on forms approved by the institutional review board at the UTHSCSA.

Acquisition of images

The images were acquired at the Research Imaging Center, UTHSCSA, using a Siemens Magnetom Trio 3 T system (Siemens, Erlangen, Germany), with a high-resolution, T_1-weighted, 3D Turbo-flash sequence with an adiabatic inversion contrast pulse with the following scan parameters: TR/TI/TE = 2100/785/3.04 ms, flip angle = 13°, voxel size (isotropic) = 0.8 mm. Each subject was scanned 7 (seven) times, consecutively, using the same protocol, and a single image was obtained by linearly coregistering these images and computing the average, allowing improvement over the signal-to-noise ratio and reducing motion artifacts (Kochunov et al., 2006).

Processing of images

Image analysis followed two separate pathways: the generation of surface representations of the cortex and the segmentation of the brain into GM, WM and CSF, in their voxel-based representation. The first part was conducted using the FreeSurfer software package

Table 1
Structure of the pedigree.

Familial relationship	Number of pairs
Self	486
Parent-offspring	164
Siblings	192
Grandparent-grandchild	14
Avuncular	298
Half-siblings	50
Double 1st cousins	1
3rd degree	530
4th degree	478
5th degree	193
6th degree	47

(Athinoula A. Martinos Center for Biomedical Imaging, Harvard University, Cambridge, MA, USA), while the second was performed using the FMRIB Software Library—FSL (Oxford Centre for Functional MRI of the Brain, University of Oxford, UK).

Surface-based analysis

The surface-based analysis followed the procedures described by Dale et al. (1999) and Fischl et al. (1999a). Images are corrected for magnetic field inhomogeneities, affine-registered to the Talairach–Tournoux atlas (Talairach and Tournoux, 1988) and skull-stripped. The voxels belonging to the WM are identified based on their locations, on their intensities and on the intensities of the neighbouring voxels. The two hemispheres are separated and the WM voxels are grouped into a mass of connected voxels using a six-neighbour connectivity scheme. A mesh of triangular faces is tightly built around the WM, using two triangles per exposed voxel face. The mesh is smoothed using an algorithm that takes into account the local intensity in the original images (Dale and Sereno, 1993), at a subvoxel resolution, using trilinear interpolation. Topological defects are corrected (Fischl et al., 2001) ensuring that the surface has the same topological properties of a sphere. A second iteration of smoothing is applied, resulting in a realistic representation of the interface between grey and white matter. This surface is referred to simply as *white surface*. The external cortical surface, which corresponds to the pia mater, is produced by nudging outwards the white surface towards a point where the tissue contrast is maximal, maintaining constraints on its smoothness and on the possibility of self-intersection (Fischl and Dale, 2000). This surface is referred to simply as the *pial surface*.

These surfaces are parcelled into smaller regions using an automated process (Fischl et al., 2004). For each subject, this is done by first homeomorphically mapping the pial surface to a spherical coordinate system (Fischl et al., 1999b), where the folding patterns are matched to an average map. An *a priori* atlas of probabilities for regions of interest is used in a Bayesian approach to establish probabilities that a given vertex belongs to a certain label. In a second, iterative step, the surface is treated as an anisotropic, non-stationary Markov random field, where for each vertex, the labels assigned to its neighbours are also considered. The labelling is iterated until no vertices change their assignments (Fischl et al., 2002, 2004). We used the regions of the atlas developed by (Desikan et al., 2006), recently modified to include the insula as an independent region of interest (Fig. 2).

Volume-based analysis

The volume-based pipeline started with skull-stripped images produced in an intermediate step of the surface-based pipeline, allowing a direct comparison between the methods. Images were segmented in GM, WM and CSF using the FAST module of FSL, which models the problem of classification into different classes as a hidden Markov random field (HMRF), an extension of hidden Markov models that assumes that the observations come from an underlying Markov random field (Kunsch et al., 1995). Thus, the assignment of a voxel to a class depends on its immediate spatial neighbours in the three-dimensional space, and the problem is treated by obtaining the maximum likelihood estimate of the parameters using an expectation-maximization (EM) algorithm (Zhang et al., 2001). The output of this HMRF-EM framework is an image where the value at each voxel corresponds to the proportion of the volume of the voxel that is occupied by a tissue class.

Estimation of these partial volume effects for each voxel is of paramount importance here, as it allows one to compute the amount of a certain class of tissue present in a region by summing the partial volume effects at each voxel of that region. The segmentation as described above operated in the images in the subject space, not transformed to a standard coordinate space. The subsequent analyses were conducted in the subject space as well, obviating the need to correct the intensities of voxels for local stretchings or shrinkages.

Combining surface-based and volume-based analyses

Voxels identified inside the space delimited by the pial and white surfaces were classified as belonging to the cortex, producing a representation of the cortical mantle in terms of voxels, tractable in a VBM-like approach. The cortex was further parcelled in the same scheme as the surface representation by assigning to each cortical voxel the same label as the closest vertex in the surfaces.

For each region defined in the voxel-based representation, the volume of grey matter was computed by integrating the partial volume effects from the images segmented using the HMRF-EM algorithm. From the surface-based representations, regional measurements for average cortical thickness, surface area and grey matter volume were obtained. Area was measured at the white surface. Global measurements for area and the grey matter volume were computed by summing the values of the parcellations, whereas a global measure of the average thickness was obtained by weighting the regional thicknesses by their corresponding surface areas. The global brain volume was produced in an intermediate step of the surface based pipeline, and includes the volumes for brain stem and cerebellum.

The cortical parcellations were projected from the surfaces into the volumetric space in a binary, not fuzzy fashion, so partial volume effects were not allowed. While this is a clearly desirable feature for the cortex as a whole, since partial volume effects were already considered within the HMRF-EM framework, this has potential to produce minor inaccuracies when computing how the grey matter volume differ across regions within the ribbon. However, these borderline voxels have the same chance of being assigned to either of two bordering regions and there is no net effect that would produce bias for any particular region.

Quantitative genetic analyses

Estimation of heritabilities

For genetic analyses we used the Sequential Oligogenic Linkage Analysis Routines — SOLAR (Department of Genetics, Southwest Foundation for Biomedical Research, San Antonio, Texas, USA). The estimates produced by SOLAR are based in a variance components method (Lange et al., 1976; Hopper and Mathews, 1982; Amos, 1994; Almasy and Blangero, 1998), in which the phenotypic variance, σ_{px}^2, for a quantitative trait x, can be considered as a sum of a genetic component σ_{gx}^2 and a residual component σ_{ex}^2,

$$\sigma_{px}^2 = \sigma_{gx}^2 + \sigma_{ex}^2 \tag{1}$$

The residual component includes all effects not accounted for by the genetic component, and is attributed to environmental effects and experimental error. The genetic component, σ_{gx}^2, can further be decomposed into an additive, σ_{ax}^2, and a dominance component, σ_{dx}^2:

$$\sigma_{px}^2 = \sigma_{ax}^2 + \sigma_{dx}^2 + \sigma_{ex}^2 \tag{2}$$

For a given pedigree, x is assumed to follow a multivariate normal distribution, and in a more generic formulation, the covariance between two non-inbred individuals i and j, drawn from a population in Hardy–Weinberg equilibrium, with random mating, is given by:

$$\Omega_{ij} = 2\Phi_{ij}\sigma_{ax}^2 + \Delta_{ij}\sigma_{dx}^2 + \delta_{ij}\sigma_{ex}^2 \tag{3}$$

in which $\Omega_{ij} = Cov_p\{x_i, x_j\}$, Φ_{ij} is the coefficient of relationship between the individuals i and j, Δ_{ij} is the probability that i and j share both alleles identically by descent and δ_{ij} is the Kronecker function. For any pair of subjects, the values for Φ_{ij} and Δ_{ij} can be calculated,
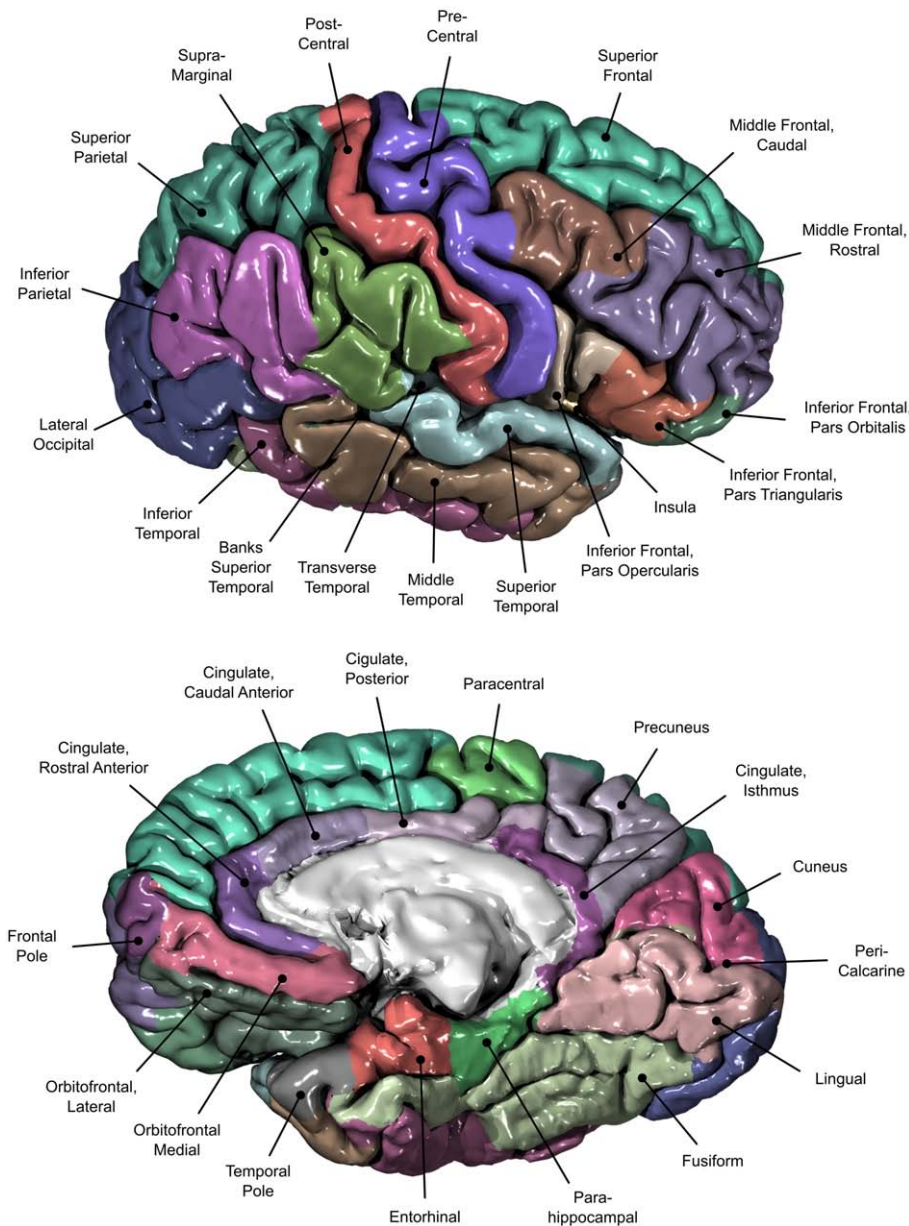
Fig. 2. The 34 cortical regions of the (Desikan et al., 2006) atlas. Some regions are buried inside sulci and cannot be fully observed.

being for siblings, for instance 1/2 and 1/4, respectively, and $1/2^k$ and 0 for most other relationships, where k is the degree of relationship (Amos, 1994). The residual term $\delta_{ij}\sigma_{ex}^2$ account for individual effects not explicitly modeled. This generic model can be extended to accommodate known environmental and other genetic effects (Hopper, 1993; Blangero et al., 2001). The broad sense heritability for the trait x is defined as the ratio $\sigma_{gx}^2/\sigma_{px}^2$ and the narrow sense heritability is defined as $\sigma_{ax}^2/\sigma_{px}^2$. The term heritability is often associated with the narrow sense (Falconer and Mackay, 1996) and is represented by h^2. To have realistic estimates, it is useful to include in the model the effects of potential confounding variables, such as age and sex. This is done by regressing the phenotype against different combinations of covariates of interest and those found to be significant remain in the model and the residuals are used to obtain maximum likelihood estimates of the variance components, instead of the actually measured raw phenotypes (Eaves et al., 1978; Barrett, 2008). For this study, we used as covariates age, sex, the product of age and sex, the square of age, as well as the product of sex with the square of age.

A statistic for hypothesis testing was computed as $\Lambda = 2(L_1 - L_0)$, in which L_0 is the maximum log-likelihood under the null hypothesis of no genetic additive effect and L_1 is the maximum log-likelihood of the alternative hypothesis (Elston and Stewart, 1971; Lange et al., 1976). Under certain conditions, Λ is distributed as a 50:50 mixture of a χ_0^2 (point mass) distribution and a χ_1^2 distribution (Self and Liang, 1987). Despite relying on a multivariate normal assumption, the variance components method is robust to departures from normality, such as skewness, although it can lead to an excess of false positives under leptokurtic conditions (Almasy and Blangero, 2008). To eschew this possibility, different transforms can be applied and, for this study, we used an inverse normal transformation based on ranks, applied directly to the phenotype measurements (Allison et al., 1999; Servin and Stephens, 2007).

Genetic and phenotypic correlations

A simple phenotypic correlation between any two traits x and y can be computed as $\rho = \text{Cov}_p\{x,y\}/(\sigma_{px}\sigma_{py})$. The $\text{Cov}_p\{x,y\} = \rho_p\sigma_{px}\sigma_{py}$ can be decomposed into genetic and residual effects, $\text{Cov}_p\{x,y\} = \text{Cov}_g$

Table 2
Relationship between measurements.

Structure pairs	Global		Regional			
	R^2	p	$\overline{R}^2$	SD	min	max
Grey Volume[a] vs. Grey Volume[b]	0.8034	2.9e-112	0.8450	0.0722	0.6523	0.9623
Grey Volume[a] vs. Surface Area	0.7881	3.3e-105	0.7844	0.0839	0.4893	0.9042
Grey Volume[a] vs. Average Thickness	0.1815	2.7e-005	0.1668	0.0919	0.0461	0.4585
Surface Area vs. Average Thickness	0.0003	5.0e-001	0.0108	0.0132	<0.0001	0.0477
Grey Volume[b] vs. Surface Area	0.5701	7.1e-044	0.6319	0.0904	0.4372	0.7913
Grey Volume[b] vs. Average Thickness	0.2850	6.6e-011	0.2035	0.0995	0.0438	0.4872

R^2 is the goodness of a linear fit; SD is the standard deviation.
[a] Measurement in the surface-based representation.
[b] Measurement in the volume-based representation.

$\{x,y\}$ + $\mathrm{Cov}_e\{x,y\}$, which can be rewritten as $\rho_p \sigma_{px} \sigma_{py} = \rho_g \sigma_{gx} \sigma_{gy} + \rho_e \sigma_{ex} \sigma_{ey}$, in which ρ_g and ρ_e are the genetic and environmental correlations, respectively. These figures represent the extent of shared residual additive genetic and environmental influences on the traits (Almasy et al., 1997). The products $\sigma_{gx} \sigma_{gy}$, as well as $\sigma_{ex} \sigma_{ey}$ are obtained by replacing, in a model similar to the Eq. (3), the elements $\Omega_{ij} = \mathrm{Cov}_p\{x_i, x_j\}$ for the covariance between the traits, $\mathrm{Cov}_p\{x_i, x_j\}$ (Falconer and Mackay, 1996; Williams et al., 1999). From the same model, partial phenotypic correlations (ρ_p), that include the effect of covariates, are obtained as:

$$\rho_p = \rho_g \sqrt{h_i^2 h_j^2} + \rho_e \sqrt{1 - h_i^2} \sqrt{1 - h_j^2} \qquad (4)$$

For this study, we computed the simple Galton–Pearson correlation coefficient between measurements and partial phenotypic correlations derived from the estimation of the heritabilities, which considers the effect of significant nuisance variables.

Results

Global measurements and their relationship

The average brain volume, including cerebellum and brain stem, was $1.136 \pm 0.121 \times 10^6$ mm^3. The grey matter volume, measured in the surface-based representation was $4.744 \pm 0.450 \times 10^5$ mm^3, which was higher than the same volume measured using the volume-based representation, for which we obtained $3.336 \pm 0.409 \times 10^5$ mm^3. We observed a higher variability on the measurements of global surface area than on average thickness. The average surface area for the whole cortex, was $1.547 \pm 0.146 \times 10^5$ mm^2, while the average cortical thickness in the same areas was 2.589 ± 0.107 mm. Cortical grey matter volumes measured by the two different methods were highly correlated (see Table 2 and Fig. 3). The correlation between the surface area and grey matter volume was also high. In contrast, thickness correlated poorly with grey matter volume and with surface area. This trend was observed globally and regionally.

The brain volume was more strongly correlated with the overall amount of grey matter measured using the surface-based method ($R^2 = 0.865$, $p = 2.5 \times 10^{-148}$) than using the volume-based method ($R^2 = 0.687$, $p = 7.9 \times 10^{-70}$). The brain volume was also highly correlated with the surface area of the cortex ($R^2 = 0.856$, $p = 1.8 \times 10^{-142}$), but was not correlated with cortical average thickness ($R^2 = 0.046$, $p = 0.153$).

Heritabilities

All global measurements were heritable. For brain volume, $h^2 = 0.696$, standard error (SE) = 0.097, $p = 6.6 \times 10^{-14}$. The heritability for the surface area was $h^2 = 0.705$, SE = 0.109, $p = 1.1 \times 10^{-11}$ and for average cortical thickness, $h^2 = 0.691$, SE = 0.119, $p = 1.7 \times 10^{-10}$. For the grey matter volume in the surface representation, we found $h^2 = 0.723$, SE = 0.099, $p = 1.6 \times 10^{-14}$ and for the voxel-based representation, $h^2 = 0.667$, SE = 0.103, $p = 2.1 \times 10^{-12}$. Table 3 shows regional heritabilities, computed using data from both hemispheres. Results for each hemisphere, separately, can be found in the Supplemental Material.

Global brain volume was a significant covariate for all heritability estimates, except for cortical thickness. When brain volume was
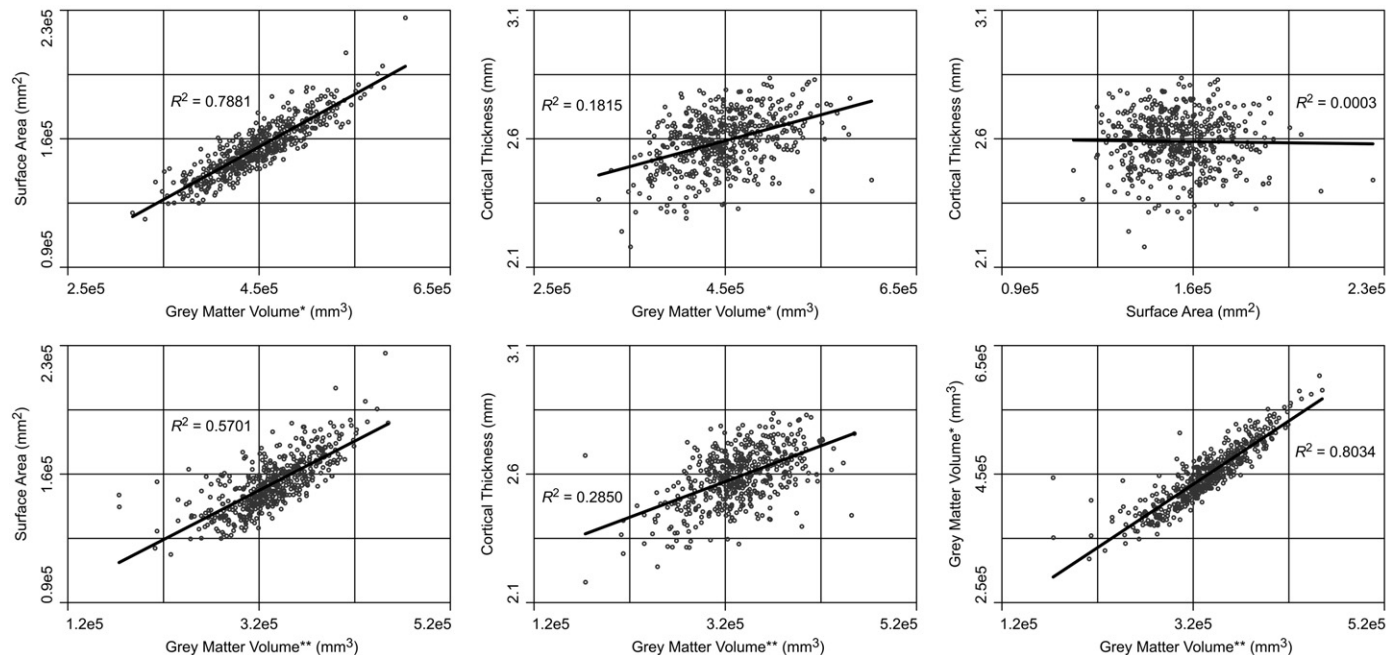

Fig. 3. Correlations between global measurements. Each point represents a pair of measurements for each subject. R^2 is the variance explained by a linear regression model. The significances are shown in Table 2. *Measurement in the surface-based representation. **Measurement in the volume-based representation.

Table 3
Heritabilities (h^2) for regional traits, both hemispheres considered.

Structure name	Average thickness			Surface area			Grey volume[a]			Grey volume[b]		
	h^2	SE	P	h^2	SE	p	h^2	SE	p	h^2	SE	p
Frontal lobe												
Superior frontal gyrus	0.46	0.13	1.1e-05	0.62	0.12	5.8e-09	0.64	0.11	5.1e-11	0.55	0.11	1.2e-08
Middle frontal gyrus; rostral division	0.48	0.12	3.1e-06	0.45	0.12	1.6e-05	0.49	0.11	4.0e-07	0.42	0.12	1.7e-05
Middle frontal gyrus; caudal division	0.53	0.12	3.0e-07	0.56	0.12	1.0e-07	0.58	0.11	3.5e-09	0.58	0.11	1.0e-09
Inferior frontal gyrus; pars opercularis	0.45	0.10	3.3e-08	0.66	0.11	3.7e-10	0.70	0.10	1.6e-12	0.69	0.10	5.6e-13
Inferior frontal gyrus; pars triangularis	0.32	0.11	6.4e-04	0.39	0.13	2.3e-04	0.43	0.13	7.9e-05	0.43	0.12	2.8e-05
Inferior frontal gyrus; pars orbitalis	0.24	0.11	6.1e-03	0.29	0.12	2.5e-03	0.19	0.10	1.9e-02	0.26	0.11	2.3e-03
Orbitofrontal cortex; lateral division	0.41	0.11	3.0e-05	0.60	0.11	8.6e-09	0.57	0.11	4.5e-09	0.58	0.11	2.3e-09
Orbitofrontal cortex; medial division	0.48	0.12	5.8e-06	0.57	0.11	1.5e-08	0.57	0.11	3.5e-09	0.53	0.11	3.5e-08
Frontal pole	0.47	0.12	5.9e-06	0.28	0.10	9.9e-04	0.34	0.11	1.0e-04	0.38	0.13	4.8e-04
Precentral gyrus	0.59	0.11	6.0e-09	0.75	0.11	4.2e-11	0.77	0.10	1.2e-13	0.66	0.10	1.1e-10
Paracentral lobule	0.59	0.13	3.0e-07	0.47	0.14	8.0e-05	0.48	0.13	7.1e-06	0.49	0.12	4.7e-06
Temporal lobe—medial aspect												
Entorhinal cortex	0.43	0.12	2.2e-05	0.44	0.12	9.9e-06	0.33	0.11	4.6e-04	0.33	0.11	5.1e-04
Parahippocampal gyrus	0.41	0.11	4.1e-05	0.64	0.11	3.3e-10	0.64	0.12	1.7e-08	0.61	0.12	1.6e-08
Temporal pole	0.26	0.10	1.7e-03	0.25	0.12	1.7e-02	0.24	0.11	1.2e-02	0.19	0.11	3.2e-02
Fusiform gyrus	0.40	0.12	2.3e-05	0.58	0.10	5.9e-10	0.61	0.10	1.3e-11	0.65	0.10	4.6e-13
Temporal lobe—lateral aspect												
Superior temporal gyrus	0.79	0.11	5.1e-13	0.64	0.11	5.8e-10	0.79	0.09	5.9e-16	0.68	0.10	3.9e-12
Middle temporal gyrus	0.42	0.12	1.5e-05	0.48	0.11	1.0e-07	0.58	0.10	1.2e-11	0.48	0.10	9.5e-09
Inferior temporal gyrus	0.57	0.11	1.0e-07	0.54	0.12	1.0e-06	0.63	0.11	1.2e-08	0.65	0.12	2.2e-09
Transverse temporal cortex	0.71	0.11	4.5e-11	0.73	0.11	3.0e-12	0.65	0.10	5.9e-12	0.70	0.10	2.1e-13
Banks of the superior temporal sulcus	0.47	0.12	7.6e-06	0.41	0.11	3.5e-06	0.49	0.11	1.4e-08	0.51	0.11	5.3e-09
Parietal lobe												
Postcentral gyrus	0.83	0.11	2.3e-13	0.58	0.11	2.8e-08	0.64	0.11	1.1e-10	0.64	0.10	3.5e-11
Supramarginal gyrus	0.55	0.12	1.0e-07	0.58	0.10	9.6e-11	0.53	0.10	3.4e-10	0.57	0.10	5.1e-12
Superior parietal cortex	0.50	0.13	3.4e-06	0.61	0.11	1.4e-08	0.56	0.12	5.0e-07	0.53	0.11	2.0e-07
Inferior parietal cortex	0.51	0.12	5.0e-07	0.59	0.11	2.7e-10	0.59	0.10	5.0e-12	0.61	0.11	2.6e-12
Precuneus cortex	0.50	0.12	1.1e-06	0.76	0.11	5.6e-14	0.75	0.10	7.0e-15	0.76	0.10	8.3e-15
Occipital lobe												
Lingual gyrus	0.56	0.13	6.0e-07	0.61	0.12	1.0e-07	0.63	0.13	1.7e-08	0.66	0.12	7.7e-10
Pericalcarine cortex	0.35	0.12	2.5e-04	0.64	0.10	1.4e-11	0.66	0.10	1.9e-11	0.64	0.10	5.3e-12
Cuneus cortex	0.50	0.13	1.8e-05	0.42	0.11	7.7e-06	0.49	0.12	9.0e-07	0.61	0.12	3.4e-09
Lateral occipital cortex	0.69	0.11	6.4e-12	0.54	0.12	2.0e-06	0.52	0.12	1.6e-06	0.49	0.12	5.0e-06
Cingulate cortex												
Rostral anterior division	0.21	0.11	1.4e-02	0.49	0.12	2.2e-06	0.59	0.12	3.8e-08	0.63	0.12	9.7e-09
Caudal anterior division	0.51	0.13	5.7e-06	0.36	0.12	1.8e-04	0.23	0.10	4.4e-03	0.27	0.11	1.7e-03
Posterior division	0.50	0.12	6.0e-07	0.61	0.11	2.2e-09	0.52	0.12	1.0e-07	0.54	0.12	1.0e-07
Isthmus division	0.70	0.11	2.1e-09	0.82	0.10	1.9e-15	0.74	0.10	9.3e-15	0.78	0.09	1.1e-15
Insular cortex	0.60	0.12	1.0e-07	0.79	0.11	3.8e-13	0.71	0.11	1.9e-12	0.78	0.10	3.1e-15

[a] Measurement in the surface-based representation.
[b] Measurement in the volume-based representation.

included together with surface area as covariate, the significance of both covariates was substantially reduced. As a general trend, even for the regional grey volume measurements, global surface area was a more significant nuisance variable. The impact on the final estimates for h^2 of including brain volume when surface area was also included was negligible. Provided that surface area, grey matter and brain volumes were found to be highly correlated (see below), our model for the regional heritabilities did not include all these potential covariates, but global surface area and average cortical thickness instead. The regional heritabilities with these covariates included is shown in Table 4 and Figs. 4 and 5.

With respect to regional variability, a simple average of the heritabilities from Table 4 shows an $\overline{h}^2 = 0.458 \pm 0.149$ for the regional surface area and $\overline{h}^2 = 0.501 \pm 0.142$ for thickness. For the grey matter volume in surface-based representation, $\overline{h}^2 = 0.489 \pm 0.1615$. For the grey matter volume in the voxel-based representation, $\overline{h}^2 = 0.482 \pm 0.146$. While none of these figures approach the global measurements, they provide a rough estimate of how the heritability varies across the brain.

Genetic and phenotypic correlations between measurements

Both surface-based and volume-based measurements of global grey matter volume were strongly correlated with the global surface area, genetically, environmentally and phenotypically (see Table 5). In contrast, cortical thickness correlated poorly and slightly negatively with surface area. Cortical thickness also correlated poorly with grey matter volume. The estimated genetic correlation was higher than the environmental (non-genetic) when the volume was computed in the surface-based representation, while the volume-based followed the opposite trend. The correlations were high between both measurements of grey matter volume.

The correlations of the brain volume with grey matter volume measured in the surface-based representation were high genetically ($\rho_g = 0.886$, $p = 5.0 \times 10^{-12}$), environmentally ($\rho_e = 0.903$, $p = 1.4 \times 10^{-13}$) and phenotypically ($\rho_p = 0.890$, p-value did not converge). Similarly, correlations with the grey matter measured in the volume-based representation were strong ($\rho_g = 0.896$, $p = 1.5 \times 10^{-11}$; $\rho_e = 0.770$, $p = 2.0 \times 10^{-3}$; $\rho_p = 0.855$, p-value did not converge). The correlations were also high between brain volume and cortical surface area ($\rho_g = 0.878$, $p = 1.3 \times 10^{-10}$; $\rho_e = 0.895$, $p = 1.9 \times 10^{-3}$; $\rho_p = 0.883$, p-value did not converge), although low and not significant between brain volume and average cortical thickness ($\rho_g = 0.161$, $p = 2.4 \times 10^{-1}$; $\rho_e = 0.006$, $p = 9.8 \times 10^{-1}$; $\rho_p = 0.113$, $p = 2.1 \times 10^{-2}$). The lack of convergence for some p-values often means extremely low significance levels, lower than the computing precision level, with an actual $p < 10^{-307}$.

While we found differences in genetic, environmental and phenotypic correlations across the cortex, generally the same trend observed for global measurements held. Remarkably, the correlations

Table 4
Heritabilities (h^2) for regional traits, both hemispheres considered, including global surface area and cortical average thickness as covariates.

Structure name	Average thickness			Surface area			Grey Volume[a]			Grey Volume[b]		
	h^2	SE	p	h^2	SE	p	h^2	SE	p	h^2	SE	p
Frontal lobe												
Superior frontal gyrus	0.63	0.12	3.3e-10	0.61	0.11	1.0e-09	0.59	0.11	7.6e-09	0.47	0.12	1.6e-05
Middle frontal gyrus; rostral division	0.29	0.13	4.2e-03	0.47	0.13	6.2e-06	0.44	0.13	5.9e-05	0.28	0.14	1.2e-02
Middle frontal gyrus; caudal division	0.46	0.12	1.8e-05	0.40	0.11	2.3e-05	0.42	0.12	1.4e-05	0.43	0.12	1.1e-05
Inferior frontal gyrus; pars opercularis	0.31	0.09	8.0e-05	0.42	0.11	4.3e-05	0.51	0.11	5.0e-07	0.54	0.11	1.0e-07
Inferior frontal gyrus; pars triangularis	0.33	0.13	2.8e-03	0.36	0.12	1.6e-04	0.37	0.13	4.3e-04	0.36	0.13	3.4e-04
Inferior frontal gyrus; pars orbitalis	0.17	0.11	5.4e-02	0.24	0.12	1.3e-02	0.20	0.12	2.9e-02	0.26	0.12	6.7e-03
Orbitofrontal cortex; lateral division	0.10	0.11	1.6e-01	0.62	0.11	1.1e-08	0.55	0.11	1.0e-07	0.57	0.12	5.0e-07
Orbitofrontal cortex; medial division	0.38	0.11	9.0e-05	0.44	0.11	5.1e-06	0.39	0.12	1.3e-04	0.34	0.12	9.4e-04
Frontal pole	0.21	0.12	3.8e-02	0.17	0.10	3.0e-02	0.18	0.11	3.0e-02	0.28	0.14	1.1e-02
Precentral gyrus	0.56	0.11	4.3e-09	0.57	0.12	1.0e-06	0.64	0.12	1.2e-08	0.46	0.14	3.3e-04
Paracentral lobule	0.53	0.12	2.4e-06	0.32	0.13	3.3e-03	0.25	0.12	1.2e-02	0.24	0.13	2.8e-02
Temporal lobe—Medial aspect												
Entorhinal cortex	0.38	0.12	9.6e-05	0.31	0.12	1.0e-03	0.23	0.12	1.3e-02	0.25	0.12	8.8e-03
Parahippocampal gyrus	0.39	0.12	9.9e-05	0.51	0.12	1.0e-06	0.46	0.14	3.0e-04	0.45	0.14	3.0e-04
Temporal pole	0.06	0.10	2.7e-01	0.27	0.12	7.7e-03	0.17	0.11	5.8e-02	0.07	0.11	2.5e-01
Fusiform gyrus	0.26	0.12	5.2e-03	0.19	0.10	1.2e-02	0.35	0.11	3.8e-05	0.45	0.10	4.0e-07
Temporal lobe – Lateral aspect												
Superior temporal gyrus	0.65	0.12	6.0e-09	0.50	0.12	7.4e-06	0.65	0.11	4.5e-10	0.52	0.12	5.0e-06
Middle temporal gyrus	0.15	0.11	7.1e-02	0.49	0.11	4.0e-07	0.52	0.11	1.0e-07	0.36	0.11	7.5e-05
Inferior temporal gyrus	0.36	0.11	1.3e-04	0.44	0.12	3.3e-05	0.51	0.12	3.7e-06	0.60	0.12	1.0e-07
Transverse temporal cortex	0.44	0.12	6.4e-05	0.67	0.11	1.5e-11	0.52	0.11	2.9e-08	0.61	0.11	3.1e-10
Banks of the superior temporal sulcus	0.28	0.12	6.3e-03	0.38	0.12	1.8e-04	0.40	0.12	4.1e-05	0.49	0.12	1.9e-06
Parietal lobe												
Postcentral gyrus	0.73	0.11	3.6e-12	0.43	0.11	3.2e-06	0.49	0.10	1.0e-07	0.54	0.10	4.3e-09
Supramarginal gyrus	0.35	0.11	4.5e-04	0.34	0.11	1.7e-04	0.33	0.11	2.8e-04	0.51	0.11	9.5e-09
Superior parietal cortex	0.36	0.12	4.8e-04	0.51	0.11	6.0e-07	0.58	0.11	1.1e-08	0.58	0.12	1.0e-07
Inferior parietal cortex	0.41	0.13	2.2e-04	0.43	0.12	3.5e-06	0.51	0.11	2.8e-08	0.64	0.12	3.7e-10
Precuneus cortex	0.17	0.12	7.0e-02	0.69	0.11	6.2e-11	0.59	0.11	3.9e-09	0.63	0.13	1.0e-07
Occipital lobe												
Lingual gyrus	0.57	0.11	5.9e-09	0.57	0.12	3.0e-07	0.64	0.12	5.6e-10	0.59	0.12	1.8e-08
Pericalcarine cortex	0.46	0.11	2.2e-06	0.68	0.10	1.9e-11	0.64	0.10	6.7e-11	0.63	0.10	2.1e-11
Cuneus cortex	0.56	0.12	1.0e-07	0.45	0.12	9.6e-06	0.53	0.11	1.0e-07	0.70	0.12	4.2e-11
Lateral occipital cortex	0.60	0.11	2.5e-08	0.54	0.11	1.7e-06	0.48	0.12	1.6e-05	0.51	0.13	2.7e-05
Cingulate cortex												
Rostral anterior division	0.12	0.10	9.8e-02	0.47	0.12	1.2e-05	0.50	0.12	1.9e-06	0.58	0.12	1.0e-07
Caudal anterior division	0.22	0.12	2.3e-02	0.23	0.10	4.5e-03	0.20	0.10	7.5e-03	0.22	0.10	5.8e-03
Posterior division	0.32	0.12	6.1e-04	0.39	0.14	1.2e-03	0.21	0.12	2.2e-02	0.20	0.13	4.1e-02
Isthmus division	0.72	0.11	7.2e-10	0.60	0.12	2.0e-07	0.51	0.11	8.0e-07	0.59	0.12	1.0e-07
Insular cortex	0.50	0.13	7.2e-06	0.76	0.13	1.7e-09	0.65	0.12	9.7e-09	0.79	0.11	6.4e-12

[a] Measurement in the surface-based representation.
[b] Measurement in the volume-based representation.

between cortical thickness and surface area were erratic and clearly non-significant for the majority of the regions. On the other hand, grey matter volume and surface area were highly and more significantly correlated and, as for the global measurements, the correlation between thickness and grey volume lied in intermediate levels between these extremes. The regional correlations are shown in Table 6.

Discussion

Relationship between surface-based and volume-based representations

Despite absolute differences between grey matter volume estimates based on each representation of the brain, the high correlation between these measurements validates each technique, and suggests that either method can be used to quantify how the global amount of grey matter varies across subjects. Strong agreement at regional level suggests that these measurements are likewise valid. However, it should be noted that regions were defined in the surface-based representation and then projected to the volumetric space, rather than directly defined from volumetric atlases or coordinate systems, as would be done in VBM-like analyses. It is possible that the agreement between surface-based and volume-based cortical parcellations might have been reduced, had these measurements been

obtained separately. Indeed, in VBM methods, the definition of regions relies heavily on the accuracy and precision of registration methods (Klein et al., 2009) and of the atlas itself.

Choice of traits for genetic studies

Since all brain traits studied were heritable to some extent, globally or regionally, it might appear that any of such traits could be of interest for genetic studies. A closer inspection, however, reveals that grey matter volume, which is a composite of two other traits (surface area and thickness), might not be the best choice. The variability for surface area measurements was higher than for the cortical thickness, implying that the variability found on grey matter volume is more closely linked to surface area than to thickness. The regional area is measured on the surface between adjacent landmarks, giving a higher, quadratic weight to tangential (horizontal) than to vertical (radial) distances, explaining why volume is more correlated with area. Furthermore, grey matter volume was genetically and environmentally correlated with surface area and, to a much lesser extent, with thickness.

While the geometric relationship between surface area and cortical thickness (Fig. 1) alone is sufficient to demonstrate their spatial orthogonality, it does not suffice to suggest their biological independence. However, the results indicate that surface area has a
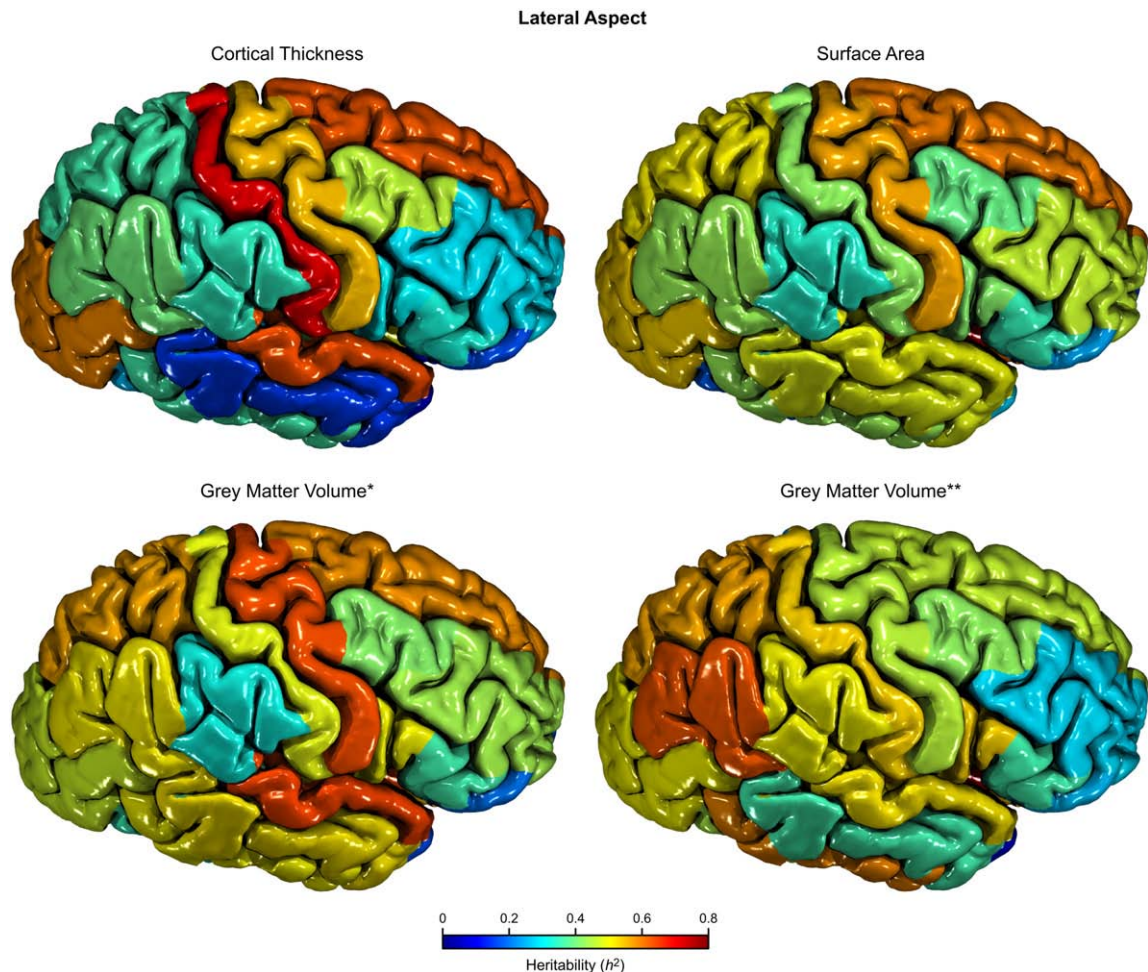
Fig. 4. Heritability (h^2) for the cortical regions using different traits, lateral aspect. *Measurement in the surface-based representation. **Measurement in the volume-based representation.

poor genetic, environmental and phenotypic correlation with cortical thickness, regionally and globally, which is evidence for the hypothesis that area and thickness are from distinct genetic origins. Based on these results, and consistent with findings from Panizzon et al. (2009), we advocate that, for imaging genetic studies, cortical thickness and surface area as separate traits of interest should be preferred over grey matter volumes.

The findings presented here also suggest that imaging methods that only provide measurements of gray matter volume may be less sensitive for gene identification than those that disentangle cortical thickness and surface area. Although VBM and similar methods have shown to be useful for a variety of non-genetic studies, their benefit for imaging genetics may be limited by not discriminating genetically independent traits as thickness and area. Moreover, studies performed in a voxel-per-voxel basis generally require that the images are aligned to a common space, which, together with the segmentation method, has the potential for introducing additional confoundings, such as misalignment, misclassification, as well as false detection of normal variants of folding patterns as focal changes on grey matter volume (Ashburner and Friston, 2007).

Yet, despite these disadvantages, volume-based techniques might have their place for the analysis of gray matter in subcortical structures and for multivariate analysis that include voxel-based functional imaging, such as functional MRI or positron emission tomography (PET). Novel algorithms to measure cortical thickness in a volumetric fashion have been recently developed (Hutton et al., 2008; Scott et al., 2009; Aganj et al., 2009; Acosta et al., 2009), which might eschew some or all of the limitations discussed above.

Advantages of these approaches include faster computing time, which might be a feature of interest for large studies or when processing capacity is scarce. These novel methods deserve a careful investigation about their potential in the context of genetic studies.

We note that the idea that cortical surface area and cortical thickness represent processes with independent genetic control is sound phylogenetically and ontogenetically. There is increasing evidence that evolution has operated more on the surface area of the brain, which variation between species is more pronounced, than on cortical thickness, which remained roughly constant in comparison (Mountcastle, 1998; Roth and Dicke, 2005; Fish et al., 2008b). Although some correlation between cortical thickness and area across species has been found (Herculano-Houzel et al., 2008), the genetic factors that control cortical thickness appear to differ from those that influence surface area. Where cortical thickness and surface area mostly determined by the same set of genes or pathways, it would be expected to find strong correlations between both, which is not the case.

From an ontogenetic standpoint, the neurons that populate the cortex migrate to their final locations (Berry and Rogers, 1965; Rakic, 1972) by following the path (scaffolding) determined the basal processes of neuroepithelial and radial cells (Kosodo and Huttner, 2009), and their final destinations, the cortical layers II–VI, are formed in an inside-out pattern (Pierani and Wassef, 2009). On the other hand, it has been hypothesised that each functional cortical column of the brain corresponds to several of what has been called "ontogenetic columns" of precursor, proliferative cells from the ventricular zone in the embryo (Rakic, 1988; Rakic et al.,
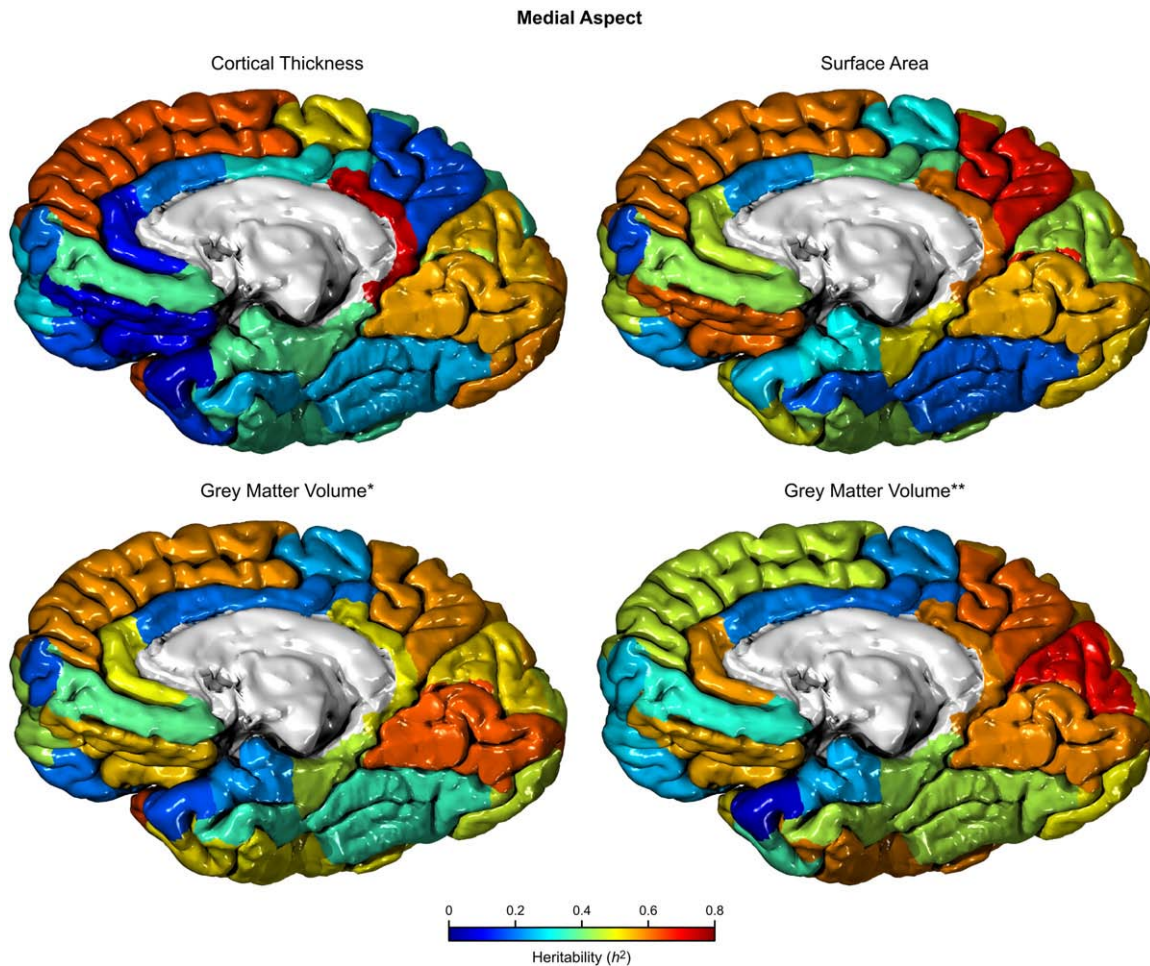
Medial Aspect

Fig. 5. Heritability (h^2) for the cortical regions using different traits, medial aspect. *Measurement in the surface-based representation. **Measurement in the volume-based representation.

2009). Experiments by Chenn and Walsh (2003) demonstrated that the brain surface area is influenced by the proliferation of these precursor cells, providing additional evidence for separate pathways that control cortical area and thickness. These hypotheses do not preclude other possible mechanisms that might underlie independent genetic control of thickness and area. The ingrowth of the thalamo-cortical and cortico-cortical fibres on the late fetal and perinatal development, and their myelination, which form an intricate network within and across cortical layers, has the potential of resulting in more pronounced horizontal than vertical growth (Kostović and Jovanov-Milošević, 2006). The migration of inter-neurons within the cortex (tangential) (Polleux et al., 2002) also has the potential to influence both thickness and area, though not necessarily on the same proportion. Moreover, the development of the neuropil of pyramidal cells (Zhang, 2004) may not be uniform over all directions, possibly growing at different rates and reaching different lengths vertically and horizontally. Therefore, the exact biological underpinnings of the genetic independence between area and thickness have a number of putative mechanisms and is a question that remains open.

Genetic influences on structural measurements

Heritability estimates for global measurements from this study are consistent with other published, twin studies (Peper et al., 2007; Schmitt et al., 2008). The estimate for brain volume included the cerebellum, which might be a source of difference if compared to reports by other groups.

Regionally, there are remarkable similarities in the distribution of genetic influences across the cortex in terms of surface area and grey matter volume, measured in the surface-based representation. For the grey matter volume in the volume-based representation, the pattern resembles the volume measured in the surface-based, although some regions follow the pattern of heritability of the thickness, suggesting that the weight of which thickness and surface area determine the volume in the voxel-based representation may be variable across the cortex.

Table 5
Genetic (ρ_g), environmental (ρ_e) and phenotypic (ρ_p) correlations between global measurements.

Structure pairs	ρ_g	ρ_e	ρ_p
Grey Volume[a] vs. Grey Volume[b]	+0.904 [9.2e-12]	+0.866 [1.7e-03]	+0.891[c]
Grey Volume[a] vs. Surface Area	+0.848 [3.1e-10]	+0.853 [3.9e-03]	+0.849[c]
Grey Volume[a] vs. Average Thickness	+0.387 [4.0e-03]	+0.235 [3.6e-01]	+0.343 [2.1e-12]
Surface Area vs. Average Thickness	−0.154 [2.9e-01]	−0.215 [4.0e-01]	−0.172 [5.0e-04]
Grey Volume[b] vs. Surface Area	+0.857 [4.8e-10]	+0.661 [1.3e-02]	+0.795[c]
Grey Volume[b] vs. Average Thickness	+0.235 [9.5e-02]	+0.428 [6.9e-02]	+0.297 [2.4e-10]

[a] Measurement in the surface-based representation.
[b] Measurement in the volume-based representation.
[c] The algorithm did not converge within the precision limit.

ARTICLE IN PRESS

Table 6

Genetic (ρ_g), environmental (ρ_e) and phenotypic (ρ_p) correlations between regional measurements for cortical thickness, surface area and grey matter volume, all measured using the surface-based representation. Global cortical average thickness and surface were included as covariates. The significance is between brackets.

Structure name	Cortical Thickness vs. Surface Area			Cortical Thickness vs. Grey Volume			Grey Volume vs. Surface Area		
	ρ_g	ρ_e	ρ_p	ρ_g	ρ_e	ρ_p	ρ_g	ρ_e	ρ_p
Frontal lobe									
Sup. frontal g.	−0.48 [1.9e-03]	−0.13 [5.4e-01]	−0.35 [6.3e-13]	−0.14 [3.8e-01]	+0.11 [5.8e-01]	−0.04 [3.9e-01]	+0.92 [4.4e-08]	+0.90 [1.5e-04]	+0.91[a]
Mid. frontal g., rostral div.	−0.45 [1.3e-01]	+0.16 [2.5e-01]	−0.05 [3.2e-01]	−0.33 [3.2e-01]	+0.41 [3.4e-03]	+0.17 [2.1e-04]	+0.96[a]	+0.94[a]	+0.95[a]
Mid. frontal g., caudal div.	+0.17 [4.1e-01]	−0.20 [1.6e-01]	−0.04 [4.4e-01]	+0.38 [6.4e-02]	+0.01 [9.6e-01]	+0.18 [1.9e-04]	+0.89[a]	+0.91[a]	+0.91[a]
Inf. frontal g., opercularis	+0.30 [1.6e-01]	−0.34 [2.5e-03]	−0.11 [2.3e-02]	+0.50 [1.1e-02]	−0.07 [5.5e-01]	+0.16 [7.3e-04]	+0.97 [8.0e-06]	+0.94 [1.1e-08]	+0.95 [7.9e-224]
Inf. frontal g., triangularis	+0.22 [4.0e-01]	−0.12 [3.8e-01]	+0.00 [9.4e-01]	+0.45 [9.8e-02]	+0.11 [4.7e-01]	+0.23 [3.9e-07]	+0.96 [8.6e-04]	+0.95 [1.2e-07]	+0.95 [1.9e-228]
Inf. frontal g., orbitalis	+0.41 [3.4e-01]	−0.14 [1.9e-01]	−0.03 [5.0e-01]	+0.71 [1.2e-01]	+0.25 [1.8e-02]	+0.33 [9.0e-14]	+0.94 [4.0e-02]	+0.87 [1.7e-10]	+0.88 [1.4e-140]
Orbitofrontal g., lat. div.	+0.06 [8.7e-01]	−0.42 [1.8e-03]	−0.23 [4.5e-07]	+0.37 [3.2e-01]	+0.18 [1.4e-01]	+0.20 [1.2e-05]	+0.92 [9.3e-08]	+0.73 [8.4e-04]	+0.84 [2.0e-114]
Orbitofrontal g., med. div.	−0.27 [1.9e-01]	−0.06 [6.6e-01]	−0.14 [2.2e-03]	+0.46 [4.3e-02]	+0.34 [6.4e-03]	+0.38 [4.4e-17]	+0.91 [2.6e-03]	+0.86 [1.0e-07]	+0.80 [4.4e-97]
Frontal pole	+0.17 [6.8e-01]	−0.19 [6.0e-02]	−0.12 [7.9e-03]	+0.41 [3.5e-01]	+0.25 [2.0e-02]	+0.28 [5.1e-10]	+0.98 [5.2e-02]	+0.86 [4.5e-12]	+0.88 [1.2e-139]
Precentral g.	+0.10 [5.4e-01]	−0.27 [1.2e-01]	−0.06 [2.0e-01]	+0.46 [2.9e-03]	+0.24 [2.1e-01]	+0.37 [4.9e-15]	+0.91 [1.1e-06]	+0.80 [1.3e-03]	+0.87 [5.9e-150]
Paracentral lobule	−0.17 [4.5e-01]	+0.23 [1.3e-01]	+0.05 [2.5e-01]	+0.39 [1.4e-01]	+0.47 [1.6e-03]	+0.42 [9.5e-19]	+0.82 [3.1e-02]	+0.94 [2.4e-09]	+0.90 [6.0e-156]
Temporal lobe—medial aspect									
Entorhinal cortex	−0.37 [1.5e-01]	−0.12 [3.4e-01]	−0.21 [5.8e-06]	+0.19 [5.3e-01]	+0.45 [2.5e-04]	+0.36 [6.0e-15]	+0.76 [3.1e-02]	+0.75 [3.3e-08]	+0.75 [1.2e-73]
Parahippocampal g.	−0.32 [1.2e-01]	−0.29 [4.9e-02]	−0.30 [1.8e-10]	+0.54 [3.2e-02]	+0.57 [3.6e-04]	+0.56 [7.0e-36]	+0.63 [4.7e-03]	+0.53 [2.5e-03]	+0.57 [8.6e-38]
Temporal pole	+0.32 [6.1e-01]	+0.11 [2.8e-01]	+0.13 [3.5e-03]	+0.25 [7.8e-01]	+0.65 [3.2e-10]	+0.60 [4.0e-49]	+1.00 [2.2e-02]	+0.76 [1.2e-09]	+0.81 [1.1e-96]
Fusiform g.	+1.00 [5.9e-03]	−0.15 [1.3e-01]	+0.09 [4.4e-02]	+0.96 [4.6e-04]	+0.22 [5.8e-02]	+0.43 [3.8e-23]	+0.97 [4.8e-04]	+0.90 [1.1e-13]	+0.90[a]
Temporal lobe—lateral aspect									
Sup. temporal g.	+0.36 [4.8e-02]	−0.38 [3.4e-02]	+0.02 [6.1e-01]	+0.71 [2.8e-06]	+0.17 [4.3e-01]	+0.51 [8.5e-28]	+0.88 [1.9e-06]	+0.79 [9.0e-05]	+0.83 [1.3e-106]
Mid. temporal g.	+0.28 [3.7e-01]	−0.17 [1.7e-01]	−0.03 [4.8e-01]	+0.44 [1.5e-01]	+0.22 [9.6e-02]	+0.27 [5.6e-09]	+0.97 [4.2e-07]	+0.88 [5.1e-06]	+0.92 [6.5e-178]
Inf. temporal g.	+0.11 [6.3e-01]	−0.09 [5.0e-01]	−0.01 [8.3e-01]	+0.47 [2.3e-02]	+0.25 [8.7e-02]	+0.35 [5.9e-14]	+0.92 [4.6e-05]	+0.90 [6.5e-07]	+0.91[a]
Trans. temporal cortex	−0.40 [1.8e-02]	+0.05 [7.7e-01]	−0.20 [2.4e-05]	+0.04 [8.2e-01]	+0.51 [8.1e-04]	+0.28 [4.5e-09]	+0.89 [8.8e-09]	+0.83 [9.3e-05]	+0.86[a]
Banks sup. temporal s.	+0.21 [4.7e-01]	+0.07 [5.6e-01]	+0.12 [1.3e-02]	+0.40 [1.4e-01]	+0.31 [1.4e-02]	+0.34 [2.1e-13]	+0.96 [6.7e-10]	+0.94 [8.6e-08]	+0.95[a]
Parietal lobe									
Postcentral g.	+0.36 [2.5e-02]	+0.03 [8.6e-01]	+0.21 [6.8e-06]	+0.81 [2.0e-08]	+0.31 [1.9e-01]	+0.61 [1.4e-45]	+0.83 [2.2e-05]	+0.91 [7.1e-09]	+0.87[a]
Supramarginal g.	−0.26 [2.9e-01]	+0.00 [9.8e-01]	−0.09 [4.6e-02]	−0.03 [9.1e-01]	+0.20 [8.8e-02]	+0.12 [7.6e-03]	+0.96 [6.0e-04]	+0.95 [1.2e-09]	+0.95[a]
Sup. parietal cortex	+0.59 [7.5e-03]	−0.19 [1.7e-01]	+0.13 [5.4e-03]	+0.71 [6.2e-04]	+0.25 [1.0e-01]	+0.44 [6.6e-22]	+0.98 [8.1e-46]	+0.86 [5.8e-06]	+0.92 [4.2e-178]
Inf. parietal cortex	+0.45 [6.4e-02]	−0.43 [2.1e-03]	−0.08 [8.6e-02]	+0.50 [1.7e-02]	−0.12 [4.1e-01]	+0.15 [1.2e-03]	+0.99 [2.3e-07]	+0.90 [1.2e-06]	+0.94 [4.7e-207]
Precuneus cortex	−0.05 [8.7e-01]	−0.31 [5.6e-02]	−0.18 [9.4e-05]	+0.03 [9.1e-01]	+0.16 [2.6e-01]	+0.10 [3.0e-02]	+0.99 [2.3e-11]	+0.78 [5.1e-03]	+0.92[a]
Occipital lobe									
Lingual gyrus	+0.16 [3.5e-01]	+0.01 [9.7e-01]	+0.09 [5.7e-02]	+0.54 [6.4e-04]	+0.38 [6.4e-02]	+0.47 [8.8e-23]	+0.91 [1.9e-11]	+0.89 [7.5e-04]	+0.90 [1.3e-155]
Pericalcarine cortex	+0.16 [3.3e-01]	+0.04 [8.2e-01]	+0.11 [2.7e-02]	+0.52 [1.7e-03]	+0.60 [6.9e-04]	+0.55 [5.9e-33]	+0.93 [1.8e-10]	+0.76 [1.6e-03]	+0.87[a]
Cuneus cortex	+0.35 [6.1e-02]	+0.09 [5.8e-01]	+0.02 [3.5e-06]	+0.70 [4.7e-05]	+0.46 [1.2e-02]	+0.59 [2.3e-39]	+0.92 [8.7e-06]	+0.89 [1.8e-06]	+0.90 [1.1e-155]
Lat. occipital cortex	−0.05 [7.7e-01]	+0.13 [4.7e-01]	+0.03 [5.8e-01]	+0.35 [4.8e-02]	+0.35 [4.7e-02]	+0.35 [1.2e-12]	+0.92 [3.1e-05]	+0.93 [1.3e-12]	+0.92 [4.0e-180]
Rostral ant. div.	+0.17 [6.3e-01]	−0.36 [2.1e-03]	−0.20 [1.3e-05]	+0.59 [8.8e-02]	+0.20 [9.4e-02]	+0.27 [1.6e-09]	+0.91 [2.1e-05]	+0.78 [1.1e-04]	+0.84 [2.7e-112]
Caudal ant. div.	+0.18 [6.1e-01]	+0.09 [3.8e-01]	+0.11 [1.5e-02]	+0.60 [1.1e-01]	+0.48 [8.1e-06]	+0.50 [5.4e-30]	+0.88 [1.8e-02]	+0.87 [1.5e-12]	+0.87 [3.5e-132]
Post. div.	−0.58 [1.5e-02]	+0.27 [6.6e-02]	−0.07 [1.2e-01]	−0.17 [5.6e-01]	+0.57 [5.4e-06]	+0.34 [5.8e-12]	+0.87 [1.1e-02]	+0.91 [9.0e-08]	+0.88 [2.2e-164]
Isthmus div.	−0.21 [1.8e-01]	−0.13 [5.9e-01]	−0.18 [2.3e-04]	+0.32 [4.5e-02]	+0.22 [2.8e-01]	+0.27 [1.5e-08]	+0.86 [5.0e-06]	+0.87 [1.3e-04]	+0.86 [2.0e-124]
Insular cortex	−0.30 [7.9e-02]	+0.10 [7.0e-01]	−0.16 [1.5e-03]	+0.21 [2.4e-01]	+0.54 [7.5e-03]	+0.35 [1.2e-12]	+0.84 [1.9e-07]	+0.73 [4.9e-02]	+0.80[a]

[a] The algorithm did not converge within the precision limit.

The heritabilities for thickness followed a distinctive pattern if compared with other traits, which corroborates to the finding that thickness is under different genetic control. While the definitions of the regions of the (Desikan et al., 2006) atlas follow macroanatomic landmarks, not cytoarchitectonic, there is evidence suggesting that there is a substantial overlap between them (Fischl et al., 2008a), and the higher regional variability suggests that regional differences on thickness might reflect underlying, regional cytoarchitectonic differences. The spatial distribution of heritabilities for surface area follows a more homogeneous pattern, particularly for the lateral aspect of the brain, suggesting a smaller degree of regional variation on genetic influences.

Results for the cortical thickness measurements are generally in agreement with the report of Lenroot et al. (2009), who parcellated the brain using a different scheme. Remarkable similarities include, for instance, high genetic effect on the thickness of the postcentral and superior temporal gyri and the very low heritability estimates for the precuneus region. There are, however, several important differences, which might be due to differences in the delimitations of the regions. For the 10 regions reported by Panizzon et al. (2009), who used a similar parcellation scheme in a sample of twins, the measurements reported here are roughly in the same range for surface area and for cortical thickness, although there are differences, possibly attributable, at least partially, to different imaging protocols and genetic analysis. The present study included subjects from both sexes and in a wider age range, which makes it more generalisable. Moreover, the findings shown here are derived from extended pedigrees, which is a more powerful and efficient study design than sibling-pairs, of which twin studies are a particular case (Blangero et al., 2003).

Since grey matter volume is a function of surface area and cortical thickness, there are no clear reasons to try to interpret regional grey matter volume differences in terms of genetic influences, particularly for the results obtained from voxel-based representations, where, as discussed, the mixture of thickness and area might follow an unknown and variable proportions across the cortical mantle.

In this report we avoided determining specific, numeric thresholds for p-values to accept or reject any hypotheses, although the numbers that support the conclusions survive a relatively assumption-free, false discovery rate (FDR) method (Benjamini and Hochberg, 1995) at $q = 0.05$. Attempts to rigorously define a threshold for family-wise error rate would have to consider the non-independence of the tests with an unknown covariance structure. We opted, instead, to clearly disclose all the p-values. Nevertheless, we underscore that, as important as the p-values themselves, are the trend that both the heritabilities and their associated significances follow, which support the conclusions hereby presented.

Acknowledgments

Appendix A. Supplementary data

Supplementary data associated with this article can be found, in the online version, at doi:10.1016/j.neuroimage.2009.12.028.

References

Acosta, O., Bourgeat, P., Zuluaga, M.A., Fripp, J., Salvado, O., Ourselin, S., Alzheimer's Disease Neuroimaging Initiative, 2009. Automated voxel-based 3D cortical thickness measurement in a combined Lagrangian–Eulerian PDE approach using partial volume maps. Med. Image Anal. 13, 730–743.

Aganj, I., Sapiro, G., Parikshak, N., Madsen, S.K., Thompson, P.M., 2009. Measurement of cortical thickness from MRI by minimum line integrals on soft-classified tissue. Hum. Brain Mapp. 30, 3188–3199.

Allison, D.B., Neale, M.C., Zannolli, R., Schork, N.J., Amos, C.I., Blangero, J., 1999. Testing the robustness of the likelihood-ratio test in a variance-component quantitative-trait loci-mapping procedure. Am. J. Hum. Genet. 65, 531–544.

Almasy, L., Blangero, J., 1998. Multipoint quantitative-trait linkage analysis in general pedigrees. Am. J. Hum. Genet. 62, 1198–1211.

Almasy, L., Blangero, J., 2008. Contemporary model-free methods for linkage analysis. Adv. Genet. 60, 175–193.

Almasy, L., Dyer, T.D., Blangero, J., 1997. Bivariate quantitative trait linkage analysis: pleiotropy versus co-incident linkages. Genet. Epidemiol. 14, 953–958.

Amos, C.I., 1994. Robust variance-components approach for assessing genetic linkage in pedigrees. Am. J. Hum. Genet. 54, 535–543.

Armstrong, E., Schleicher, A., Omran, H., Curtis, M., Zilles, K., 1995. The ontogeny of human gyrification. Cereb. Cortex 1, 56–63.

Ashburner, J., Friston, K.J., 2000. Voxel-based morphometry—the methods. NeuroImage 11, 805–821.

Ashburner, J., Friston, K.J., 2007. Voxel-based morphometry. In: Friston, K.J., Ashburner, J.T., Kiebel, S.J., Nichols, T.E., Penny, W.D. (Eds.), Statistical Parametric Mapping: The Analysis of Functional Brain Images. Academic Press, pp. 339–351.

Baaré, W.F.C., Hulshoff Pol, H.E., Boomsma, D.I., Posthuma, D., de Geus, E.J.C., Schnack, H. G., van Haren, N.E.M., van Oel, C.J., Kahn, R.S., 2001. Quantitative genetic modeling of variation in human brain morphology. Cereb. Cortex 11, 816–824.

Barrett, J.H., 2008. Measuring the effects of genes and environment on complex traits. Methods Mol. Med. 141, 55–69.

Benjamini, Y., Hochberg, Y., 1995. Controlling the false discovery rate: a practical and powerful approach to multiple testing. J. R. Stat. Soc. B 57, 289–300.

Berry, M., Rogers, A.W., 1965. The migration of neuroblasts in the developing cerebral cortex. J. Anat. 99, 691–709.

Blangero, J., Williams, J.T., Almasy, L., 2001. Variance component methods for detecting complex trait loci. Adv. Genet. 42, 151–181.

Blangero, J., Williams, J.T., Almasy, L., 2003. Novel family-based approaches to genetic risk in thrombosis. J. Thromb. Haemost. 1, 1391–1397.

Bullmore, E.T., Suckling, J., Overmeyer, S., Rabe-Hesketh, S., Taylor, E., Brammer, M.J., 1999. Global, voxel, and cluster tests, by theory and permutation for a difference between two groups of structural MR images of the brain. IEEE Trans. Med. Imag. 18, 32–42.

Chenn, A., Walsh, C.A., 2003. Increased neuronal production, enlarged forebrains and cytoarchitectural distortions in beta-catenin overexpressing transgenic mice. Cereb. Cortex 13, 599–606.

Dale, A.M., Sereno, M.I., 1993. Improved localization of cortical activity by combining EEG and MEG with MRI cortical surface reconstruction. J. Cogn. Neurosci. 5, 162–176.

Dale, A.M., Fischl, B., Sereno, M.I., 1999. Cortical surface-based analysis I: Segmentation and surface reconstruction. NeuroImage 9, 179–194.

Desikan, R.S., Ségonne, F., Fischl, B., Quinn, B.T., Dickerson, B.C., Blacker, D., Buckner, R.L., Dale, A.M., Maguire, R.P., Hyman, B.T., Albert, M.S., Killiany, R.J., 2006. An automated labeling system for subdividing the human cerebral cortex on mri scans into gyral based regions of interest. NeuroImage 31, 968–980.

Eaves, L.J., Last, K.A., Young, P.A., Martin, N.G., 1978. Model-fitting approaches to the analysis of human behaviour. Heredity 41, 249–320.

Elston, R.C., Stewart, J., 1971. A general model for the genetic analysis of pedigree data. Hum. Hered. 21, 523–542.

Falconer, D.S., Mackay, T.F., 1996. Introduction to Quantitative Genetics. Pearson-Prentice Hall, Harlow, Essex, UK.

Fischl, B., Dale, A.M., 2000. Measuring the thickness of the human cerebral cortex from magnetic resonance images. Proc. Natl. Acad. Sci. U. S. A. 97, 11050–11055.

Fischl, B., Sereno, M.I., Dale, A.M., 1999a. Cortical surface-based analysis II: inflation, flattening, and a surface-based coordinate system. NeuroImage 9, 195–207.

Fischl, B., Sereno, M.I., Tootell, R.B., Dale, A.M., 1999b. High-resolution intersubject averaging and a coordinate system for the cortical surface. Hum. Brain Mapp. 8, 272–284.

Fischl, B., Liu, A., Dale, A.M., 2001. Automated manifold surgery: constructing geometrically accurate and topologically correct models of the human cerebral cortex. IEEE Trans. Med. Imaging 20, 70–80.

Fischl, B., Salat, D.H., Busa, E., Albert, M., Dieterich, M., Haselgrove, C., van der Kouwe, A., Killiany, R., Kennedy, D., Klaveness, S., Montillo, A., Makris, N., Rosen, B., Dale, A.M., 2002. Whole brain segmentation: automated labeling of neuroanatomical structures in the human brain. Neuron 33, 341–355.

Fischl, B., van der Kouwe, A., Destrieux, C., Halgren, E., Ségonne, F., Salat, D.H., Busa, E., Seidman, L.J., Goldstein, J., Kennedy, D., Caviness, V., Makris, N., Rosen, B., Dale, A.M., 2004. Automatically parcellating the human cerebral cortex. Cereb. Cortex 14, 11–22.

Fischl, B., Rajendran, N., Busa, E., Augustinack, J., Hinds, O., Yeo, B.T., Mohlberg, H., Amunts, K., Zilles, K., 2008a. Cortical folding patterns and predicting cytoarchitecture. Cereb. Cortex 97, 11050–11055.

Fish, J.L., Dehay, C., Kennedy, H., Huttner, W.B., 2008b. Making bigger brains—the evolution of neural-progenitor-cell division. J. Cell Sci. 121, 2783–2793.

Geschwind, D.H., Miller, B.L., DeCarli, C., Carmelli, D., 2002. Heritability of lobar brain volumes in twins supports genetic models of cerebral laterality and handedness. Proc. Natl. Acad. Sci. U. S. A. 99, 3176–3181.

Glahn, D.C., Thompson, P.M., Blangero, J., 2007. Neuroimaging endophenotypes: strategies for finding genes influencing brain structure and function. Hum. Brain Mapp. 28, 488.

Goldman, A.L., Pezawas, L., Mattay, V.S., Fischl, B., Verchinski, B.A., Chen, Q., Weinberger, D.R., Meyer-Lindenberg, A., 2009. Widespread reductions of cortical thickness in schizophrenia and spectrum disorders and evidence of heritability. Arch. Gen. Psychiatry 66, 467–477.

Goldman, A.L., Pezawas, L., Mattay, V.S., Fischl, B., Verchinski, B.A., Zoltick, B., Weinberger, D.R., Meyer-Lindenberg, A., 2008. Heritability of brain morphology related to schizophrenia: a large-scale automated magnetic resonance imaging segmentation study. Biol. Psychiatry 63, 475–483.

Good, C.D., Johnsrude, I.S., Ashburner, J., Henson, R.N., Friston, K.J., Frackowiak, R.S., 2001. A voxel-based morphometric study of ageing in 465 normal adult human brains. NeuroImage 14, 21–36.

Gottesman, I.I., Gould, T.D., 2003. The endophenotype concept in psychiatry: etymology and strategic intentions. Am. J. Psychiatry 160, 636–645.

Gottesman, I.I., Shields, J., 1967. A polygenic theory of schizophrenia. Proc. Natl. Acad. Sci. U. S. A. 58, 199–205.

Herculano-Houzel, S., Collins, C.E., Wong, P., Kaas, J.H., Lent, R., 2008. The basic nonuniformity of the cerebral cortex. Proc. Natl. Acad. Sci. U. S. A. 105, 12593–12598.

Hofman, M.A., 1985. Size and shape of the cerebral cortex in mammals. I. The cortical surface. Brain Behav. Evol. 27, 28–40.

Honea, R.A., Meyer-Lindenberg, A., Hobbs, K.B., Pezawas, L., Mattay, V.S., Egan, M.F., Verchinski, B., Passingham, R.E., Weinberger, D.R., Callicott, J.H., 2008. Is gray matter volume an intermediate phenotype for schizophrenia? A voxel-based morphometry study of patients with schizophrenia and their healthy siblings. Biol. Psychiatry 63, 465–474.

Hopper, J.L., 1993. Variance components for statistical genetics: applications in medical research to characteristics related to human diseases and health. Stat. Methods Med. Res. 2, 199–223.

Hopper, J.L., Mathews, J.D., 1982. Extensions to multivariate normal models for pedigree analysis. Ann. Hum. Genet. 46, 373–383.

Hutton, C., Vita, E.D., Ashburner, J., Deichmann, R., Turner, R., 2008. Voxel-based cortical thickness measurements in MRI. NeuroImage 40, 1701–1710.

Klein, A., Andersson, J., Ardekani, B.A., Ashburner, J., Avants, B., Chiang, M.C., Christensen, G.E., Collins, D.L., Gee, J., Hellier, P., Song, J.H., Jenkinson, M., Lepage, C., Rueckert, D., Thompson, P., Vercauteren, T., Woods, R.P., Mann, J.J., Parsey, R.V., 2009. Evaluation of 14 nonlinear deformation algorithms applied to human brain MRI registration. NeuroImage 46, 786–802.

Kochunov, P., Lancaster, J.L., Glahn, D.C., Purdy, D., Laird, A.R., Gao, F., Fox, P.T., 2006. Retrospective motion correction protocol for high-resolution anatomical MRI. Hum. Brain Mapp. 27, 957–962.

Kosodo, Y., Huttner, W.B., 2009. Basal process and cell divisions of neural progenitors in the developing brain. Dev. Growth Differ. 51, 251–261.

Kostović, I., Jovanov-Milošević, N., 2006. The development of cerebral connections during the first 20–45 weeks' gestation. Semin. Fetal Neonatal Med. 11, 415–422.

Kunsch, H., Geman, S., Kehagias, A., 1995. Hidden Markov random fields. Ann. Appl. Probab. 5, 577–602.

Lange, K., Westlake, J., Spence, M.A., 1976. Extensions to pedigree analysis. III. Variance components by the scoring method. Ann. Hum. Genet. 39, 485–491.

Lenroot, R.K., Schmitt, J.E., Ordaz, S.J., Wallace, G.L., Neale, M.C., Lerch, J.P., Kendler, K.S., Evans, A.C., Giedd, J.N., 2009. Differences in genetic and environmental influences on the human cerebral cortex associated with development during childhood and adolescence. Hum. Brain Mapp. 30, 163–174.

Mangin, J.-F., Frouin, V., Bloch, I., Regis, J., Lopes-Krabe, J., 1995. From 3D MR images to structural representations of the cortex topography using topology preserving deformations. J. Math. Imaging Vis. 5, 297–318.

McDonald, C., Marshall, N., Sham, P.C., Bullmore, E.T., Schulze, K., Chapple, B., Bramon, E., Filbey, F., Quraishi, S., Walshe, M., Murray, R.M., 2006. Regional brain morphometry in patients with schizophrenia or bipolar disorder and their unaffected relatives. Am. J. Psychiatry 163, 478–487.

Mountcastle, V.P., 1998. Perceptual Neuroscience: The Cerebral Cortex. Harvard University Press, Cambridge, MA, USA.

Panizzon, M.S., Fennema-Notestine, C., Eyler, L.T., Jernigan, T.L., Prom-Wormley, E., Neale, M., Jacobson, K., Lyons, M.J., Grant, M.D., Franz, C.E., Xian, H., Tsuang, M., Fischl, B., Seidman, L., Dale, A., Kremen, W.S., 2009. Distinct genetic influences on cortical surface area and cortical thickness. Cereb. Cortex 19, 2728–2735.

Peper, J.S., Brouwer, R.M., Boomsma, D.I., Kahn, R.S., Hulshoff Pol, H.E., 2007. Genetic influences on human brain structure: a review of brain imaging studies in twins. Hum. Brain Mapp. 28, 464.

Pierani, A., Wassef, M., 2009. Cerebral cortex development: from progenitors to patterning to neocortical size during evolution. Dev. Growth Differ. 51, 325–342.

Polleux, F., Whitford, K.L., Dijkhuizen, P.A., Vitalis, T., Ghosh, A., 2002. Control of cortical interneuron migration by neurotrophins and PI3-kinase signaling. Development 129, 3147–3160.

Rakic, P., 1972. Mode of cell migration to the superficial layers of the fetal monkey neocortex. J. Comp. Neurol. 145, 61–84.

Rakic, P., 1988. Specification of cerebral cortical areas. Science 241, 170–176.

Rakic, P., Ayoub, A.E., Breunig, J.J., Dominguez, M.H., 2009. Decision by division: making cortical maps. Trends Neurosci. 32, 291–301.

Rao, D.C., 2008. An overview of the genetic dissection of complex traits. Adv. Genet. 60, 1–34.

Roth, G., Dicke, U., 2005. Evolution of the brain and intelligence. Trends Cogn. Sci. 9, 250–257.

Schmitt, J.E., Eyler, L.T., Giedd, J.N., Kremen, W.S., Kendler, K.S., Neale, M.C., 2008. Review of twin and family studies on neuroanatomic phenotypes and typical neurodevelopment. Twin Res. Hum. Genet. 10, 683–694.

Scott, M.L.J., Bromiley, P.A., Thacker, N.A., Hutchinson, C.E., Jackson, A., 2009. A fast, model-independent method for cerebral cortical thickness estimation using MRI. Med. Image Anal. 13, 269–285.

Self, S.G., Liang, K.-Y., 1987. Asymptotic properties of maximum likelihood estimators and likelihood ratio tests under nonstandard conditions. J. Am. Stat. Assoc. 82, 605–610.

Servin, B., Stephens, M., 2007. Imputation-based analysis of association studies: candidate regions and quantitative traits. PLoS Genet. 3.

Talairach, J., Tournoux, P., 1988. Co-Planar Stereotaxic Atlas of the Human Brain: 3-D Proportional System: An Approach to Cerebral Imaging. Thieme, Stuttgart, Germany.

Thompson, P.M., Cannon, T.D., Narr, K.L., van Erp, T., Poutanen, V.P., Huttunen, M., Lönnqvist, J., Standertskjöld-Nordenstam, C.G., Kaprio, J., Khaledy, M., Dail, R., Zoumalan, C.I., Toga, A.W., 2001. Genetic influences on brain structure. Nat. Neurosci. 4, 1253.

van der Schot, A.C., Vonk, R., Brans, R.G., van Haren, N.E., Koolschijn, P.C., Nuboer, V., Schnack, H.G., van Baal, G.C., Boomsma, D.I., Nolen, W.A., Hulshoff-Pol, H.E., Kahn, R.S., 2009. Influence of genes and environment on brain volumes in twin pairs concordant and discordant for bipolar disorder. Arch. Gen. Psychiatry 66, 142–151.

van Essen, D.C., Drury, H.A., Joshi, S., Miller, M.I., 1998. Functional and structural mapping of human cerebral cortex: Solutions are on the surfaces. Proc. Natl. Acad. Sci. U. S. A. 95, 788–795.

van Essen, D.C., Lewis, J.W., Drury, H.A., Hadjikhani, N., Tootell, R.B.H., Bakircioglu, M., Miller, M.I., 2001. Mapping visual cortex in monkeys and humans using surface-based atlases. Vis. Res. 41, 1359–1378.

Williams, J.T., van Eerdewegh, P., Almasy, L., Blangero, J., 1999. Joint multipoint linkage analysis of multivariate qualitative and quantitative traits. I. Likelihood formulation and simulation results. Am. J. Hum. Genet. 65, 1134.

Winkler, A.M., Kochunov, P., Fox, P.T., Duggirala, R., Almasy, L., Blangero, J., Glahn, D.C., 2009. Heritability of volume, surface area and cortical thickness for anatomically defined central brain regions estimated in a large extended pedigree. NeuroImage 47, s162 URL http://www.glahngroup.org/Members/anderson/publications/HBM2009_h2_poster.pdf.

Wojczynski, M.K., Tiwari, H.K., 2008. Definition of phenotype. Adv. Genet. 60, 75–105.

Wright, I.C., McGuire, P.K., Poline, J.-B., Travere, J.M., Murray, R.M., Frith, C.D., Frackowiak, R.S.J., Friston, K.J., 1995. A voxel-based method for the statistical analysis of gray and white matter density applied to schizophrenia. NeuroImage 2, 244.

Zhang, Y., Brady, M., Smith, S., 2001. Segmentation of brain MR images through a hidden Markov random field model and the expectation-maximization algorithm. IEEE Trans. Med. Imaging 20, 45–57.

Zhang, Z.-W., 2004. Maturation of layer V pyramidal neurons in the rat prefrontal cortex: intrinsic properties and synaptic function. J. Neurophysiol. 91, 1171–1182.